

# Tracking a nanosize magnetic particle using a magnetic force microscope

Dimitar Baronov, Sean B. Andersson and John Baillieul

**Abstract**—A scheme for tracking nano-sized magnetic particles using a magnetic force microscope (MFM) is introduced. The stray magnetic field of the particle induces a shift in the phase of the oscillation of the MFM tip. The magnitude of this shift depends on the distance between the tip and the particle and can be expressed as a spatial field. We present a control law which steers the tip to a level set of this field. The approach is based on the previous work of two of the authors on a novel method for mapping unknown potential fields using sensor-enabled mobile robots. Because the method involves geometric properties of the field and its domain, it is not surprising that it can be applied to problems where the characteristic length scales are small. Additionally, we introduce to the original control law an adaptive term to compensate for uncertainties in the parameter values in the model of the magnetic force. The efficacy of this approach is illustrated through simulation. This approach to tracking will provide the capability to investigate the dynamics of single molecules with a higher resolution (in both space and time) than is currently possible.

## I. INTRODUCTION

In this paper we introduce a scheme for tracking single magnetic nanoparticles using a magnetic force microscope (MFM). We achieve tracking by building upon results of two of the authors for the automated tracking of a level set of a potential field [1]. In an MFM, a magnetized tip at the end of a cantilevered beam is brought in proximity to a sample and then driven into oscillation. The stray magnetic field of the sample gives rise to a shift in the phase of the oscillation. It is this shift that defines the potential field. We show that for a single particle, this field has closed level sets, and using this fact, we develop a control law which converges to a desired phase shift. As the particle moves in the sample plane, the level sets also move. This gives rise to the desired tracking.

Magnetic particles of sizes ranging from  $2\ \mu\text{m}$  down to a few nanometers are commonly used to label, manipulate, and interact with biological molecules. This labeling is used in a variety of ways including as a means to separate specific particles for subsequent analysis, to enable targeted drug delivery, as a contrast agent for magnetic resonance imaging, as powerful heat sources useful for the destruction of tumour cells, and as a detector of single molecules and of the interactions between molecules [2]-[5]. We are interested in using an MFM to monitor the motion of a magnetic nanoparticle and thereby reveal information on the dynamics of the molecule to which it is attached.

The MFM is a special type of atomic force microscope in which the tip is a ferromagnetic probe. The resolution and sensitivity depend largely on the geometry and magnetic

properties of the probe. Resolution on the order of 100 nm is easily achievable [6] and recent results have yielded a resolution as fine as 10 nm [7], [8]. The technique is easy to perform and can be operated in a variety of physical environments, including in liquid. These properties make MFM a useful tool for non-invasive imaging of molecular structures with a resolution better than that achievable with optical techniques.

The typical approach to exploring dynamic phenomena using scanning probe microscopy techniques such as MFM is through the acquisition of a series of images followed by an analysis of the image set. However, typical times to acquire a single frame are on the order of several seconds to many minutes. This greatly limits the applicability of the technique. As a result there have been many efforts on improving the speed of AFM (and thereby the related technologies such as MFM) while maintaining image quality. These approaches have included redesigning the actuator to achieve higher bandwidth [9] and applications of modern control [10]-[13]. Recently one of the authors has proposed a new approach which reduces the number of scan points to be acquired by taking advantage of the structure of the sample [14], [15]. Here we take advantage of this general non-raster approach and develop a scheme to track the motion of a molecule *directly* by first labeling it with a magnetic nanoparticle and then tracking that nanoparticle with the microscope.

## II. MFM - INTERACTION MODEL

The MFM is a scanning probe microscope in which a magnetized probe at the end of a cantilever interacts with the magnetic field of the sample. In the most common imaging mode the probe tip is brought near (typically 25-150 nm) the sample surface and the cantilever is driven into a low-amplitude oscillation. The interaction between the tip and the sample leads to a detectable shift in the phase of the oscillation (see (4) below). An image of this interaction is obtained by scanning the probe with respect to the sample.

### A. Force to phase model

In the following we derive the dependence of the phase shift on the external force applied to the cantilever. For more details see [6]. The basic setup is pictured in Fig. 1. The tip motion is given with respect to a fixed coordinate frame whose  $(x, y)$  axes lie in the sample plane. The amplitude of oscillation is typically between 10-100 Å. This is small with respect to the typical length of a cantilever and therefore it is assumed that the tip motion is purely in the  $z$  direction. Under this assumption, the dynamics of the tip can be written as:

$$\frac{d^2 z_{tip}}{dt^2} + \frac{\omega_0}{Q} \frac{dz_{tip}}{dt} + \omega_0^2 (z_{tip} - z_0) = \delta_0 \omega_0^2 \cos(\omega t), \quad (1)$$

This work was supported in part by ODDR&E MURI01 DAAD19-01-1-0465 to Boston University and the Center for Networked Communicating Control Systems, by NSF ITR Program DMI-0330171, and by NSF DBI-0649823

D. Baronov, S.B. Andersson and J. Baillieul are with the Department of Aerospace and Mechanical Engineering, Boston University, Boston, MA, 02215. {baronov, sanderss, johnb}@bu.edu

where  $z_{tip}$  is the distance between the probe and the sample plane,  $z_0$  is the probe-sample distance at zero oscillation amplitude,  $\omega_0$  is the natural frequency of the cantilever,  $Q$  is the quality factor of the vibration,  $\omega$  is the driving force frequency and  $\delta_0$  is the amplitude of displacement at the clamped end of the cantilever. In the absence of an external force, the phase response of the system can be shown to be:

$$\phi = \tan^{-1} \left( \frac{\omega\omega_0}{Q(\omega_0^2 - \omega^2)} \right). \quad (2)$$

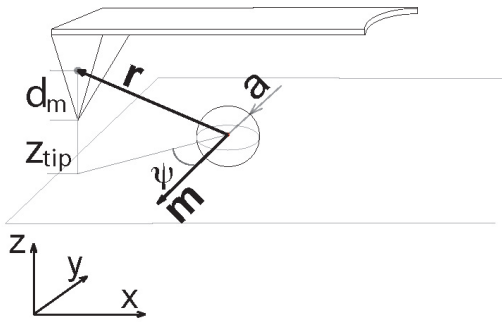


Fig. 1. MFM setup. Here  $\mathbf{r}$  is the position vector of the effective dipole moment relative to the particle center,  $d_m$  is the distance of the effective magnetic dipole moment relative to the end of the tip,  $z_{tip}$  is the distance from the end of the tip to the sample plane containing the center of the magnetic particle,  $a$  is the radius of the particle,  $\mathbf{m}$  is the particle's magnetization vector, and  $\psi$  is the angle between the projections of  $\mathbf{r}$  and  $\mathbf{m}$  on the sample plane.

The magnetic force acting on the tip is a nonlinear function of both  $\frac{dz_{tip}}{dt}$  and  $z_{tip}$ . Because of the small amplitude of the oscillation, we use the linearization of the interaction force, as in [6],

$$F \left( z_{tip}, \frac{dz_{tip}}{dt} \right) = F(z_0, 0) + \left. \frac{\partial F}{\partial z_{tip}} \right|_{z_{tip}=z_0} (z_{tip} - z_0).$$

Introducing this term as a driving force in (1) reveals that the effect of the external magnetic force is to modify the spring constant according to whether the force is attractive or repelling. This leads to a shift in the natural frequency of the cantilever, resulting in the effective natural frequency

$$\tilde{\omega}_0 = \omega_0 \sqrt{1 - \frac{1}{k} \frac{dF}{dz_{tip}}}. \quad (3)$$

This in turn leads to a change in the phase of the oscillation  $\Delta\phi = \phi - \tilde{\phi}$ . The tip is driven near its original natural frequency  $\omega_0$  and thus, from (2),  $\phi = \frac{\pi}{2}$ . Using this result and replacing  $\omega_0$  with  $\tilde{\omega}_0$  in (2) yields

$$\Delta\phi = \tan^{-1} \left( -\frac{Q \frac{1}{k} \frac{dF}{dz_{tip}}}{\sqrt{1 - \frac{1}{k} \frac{dF}{dz_{tip}}}} \right). \quad (4)$$

### B. Magnetic force model

The magnetic force acting on the magnetic tip can be expressed as the convolution of the magnetization of the tip,  $\mathbf{M}_{tip}$ , and the stray field of the sample,  $\mathbf{H}_s$  [16]:

$$\mathbf{F}(\mathbf{r}_{tip}) = \mu_0 \int_{tip} (\mathbf{M}_{tip}(\mathbf{r}') \cdot \nabla_{\mathbf{r}_{tip}}) \mathbf{H}_s(\mathbf{r}_{tip} - \mathbf{r}') d\mathbf{r}',$$

where  $\mathbf{r}_{tip}$  is the position vector to the tip. To solve for the magnetic force, the integral must be determined (numerically) given the geometry of the tip and the knowledge of the sample. To avoid this, the tip can be abstracted as a magnetic dipole. This yields the following simpler expression for the force field [17]:

$$\mathbf{F}(\mathbf{r}_{tip}) = \mu_0 \mathbf{m} \cdot \nabla \mathbf{H}_s(\mathbf{r}_{tip} + \Delta\mathbf{r}_m), \quad (5)$$

where  $\mathbf{m}$  is the effective dipole moment and  $\Delta\mathbf{r}_m = \{0, 0, d_m\}^T$  is the position of the effective magnetic dipole moment relative to the end of the tip (see Fig. 1). We note that more sophisticated models are available for which the tip is treated as a combination of a magnetic monopole and a magnetic dipole [6]. However the introduction of the term representing the monopole in (5) does not lead to large quantitative or qualitative differences in the model and is often omitted.

MFM tips are typically manufactured such that their magnetization vector lies along the  $z$  direction. Using this in (5) yields

$$\frac{dF}{dz} = \nabla \mathbf{F} \cdot \hat{\mathbf{z}} = \mu_0 m_z \left. \frac{\partial^2 H_z}{\partial z^2} \right|_{z=z_0+d_m}, \quad (6)$$

where  $\mathbf{m} = \{0, 0, m_z\}^T$  and  $z_0$  is the nominal distance between the tip and the sample plane.

The magnetic beads which we intend to track are small, uniformly magnetized spheres. The stray magnetic field from such a particle is given by:

$$\mathbf{H}_s(\mathbf{r})_{r>a} = \frac{1}{4\pi} \left[ -\frac{\mathbf{m}_s}{r^3} + \frac{3(\mathbf{m}_s \cdot \mathbf{r})\mathbf{r}}{r^5} \right], \quad (7)$$

where  $\mathbf{r}$  is a radius vector whose origin coincides with the center of the sphere,  $a$  is the radius of the sphere and  $\mathbf{m}_s$  is the equivalent magnetic moment of the sphere. This moment depends both on the material magnetization,  $M$ , and the volume of the sphere:

$$\mathbf{m}_s = \frac{4}{3}\pi a^3 M \hat{\mathbf{n}}, \quad (8)$$

where  $\hat{\mathbf{n}}$  is the unit vector specifying the orientation of the magnetization. Assuming that  $\hat{\mathbf{n}}$ , the magnetization vector of the sphere, lies in the sample plane, (5) and (7) lead to:

$$\frac{\partial^2 H_z}{\partial z^2} = 5a^3 M \frac{z r_{xy} \cos \psi (-3r_{xy}^2 + 4z^2)}{r^9}. \quad (9)$$

Here  $\mathbf{r}_{xy}$  is the projection of  $\mathbf{r}$  into the sample plane,  $r_{xy}$  is the Euclidean length of  $\mathbf{r}_{xy}$  and  $\psi$  is the angle between  $\mathbf{r}$  and  $\mathbf{r}_{xy}$  (see Fig. 1).

Inserting (9) into (6) yields the  $z$ -component of the force gradient which in turn yields the phase shift from (4). Fig. 2 shows how this phase difference evolves as a function of  $r_{xy} \cos \psi$  given that  $\mathbf{r}_{xy}$  is parallel to  $\hat{\mathbf{n}}$  (i.e.  $\cos \psi = \pm 1$ ). The evolution is shown for several values of  $z_0$  and for realistic values for the parameters in (4), (6), (9) and (10).

One of the prime sources of noise in force microscopy which limits the resolution is the thermal motion of the cantilever [18]. The standard deviation of this noise is given by

$$\sigma_n = \frac{1}{\delta_{rms}} \sqrt{\frac{2k_b T B}{\omega_0 Q}}, \quad (10)$$

where  $\delta_{rms}$  is the root mean-square amplitude of the tip,  $k_b$  is Boltzmann's constant,  $T$  is the ambient temperature and  $B$  is the bandwidth of the measurements. Using the linearization of (4), we can propagate the noise into the phase shift. The corresponding dispersion is plotted in Fig. 2 against the phase shift induced from the magnetic particle.

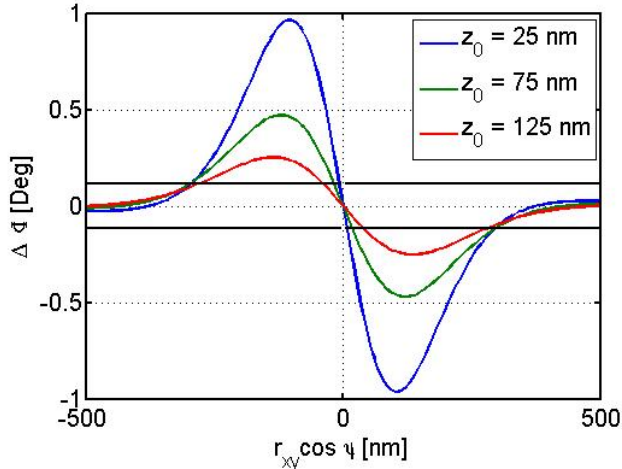


Fig. 2. The phase shift as a function of  $r_{x,y} \cos \psi$  ( $\cos \psi = \pm 1$ ) for three different values of  $z_0$  and the standard deviation of the error due to thermal noise. The following values of the parameters are used:  $Q = 500$ ,  $T = 300$  K,  $\omega_0 = 75$  Hz,  $B = 100$  Hz,  $\delta_{rms} = 10$  nm,  $k = 1.5$  N/m,  $m_z = 5.1 \times 10^{-15}$  A/m<sup>2</sup>,  $d_m = 300$  nm (The last two values are experimentally determined in [19]),  $M = 480 \times 10^3$  A/m (which is the saturation magnetization of magnetite -  $Fe_2O_3$ ) and  $a = 25$  nm.

Fig. 3 shows a simulated raster scan image of the phase shift in the region around the particle, based on the developed model. The magnetic dipole of the particle leads to two regions, one repelling and one attracting, corresponding to  $\cos \psi > 0$  and  $\cos \psi < 0$ . As shown in Fig. 4, the shape of these regions depends on the orientation of  $\hat{n}$ . As this normal vector rotates out of the sample plane, one of the poles becomes dominant at the expense of the other.

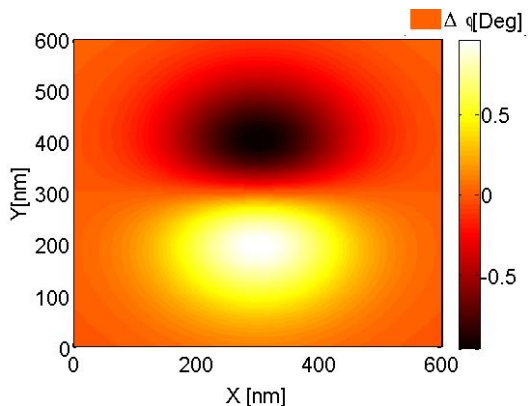


Fig. 3. The phase shift image. The tip-sample separation was set to  $z_0 = 25$  nm.

### III. TIP CONTROL

#### A. Tracking a magnetic particle as level set tracking

The objective is to generate a stable control law which will enable the tip to track the motion of the magnetic particle.

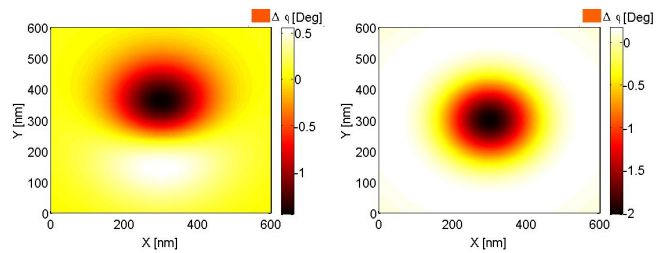


Fig. 4. The phase shift for the case when  $\hat{n}$  lies out of the sample plane by  $30^\circ$  (left image) and  $90^\circ$  (right image). The tip-sample separation was set to  $z_0 = 25$  nm.

As described below, this is achieved by tracking the level set of a potential field defined by the phase shift.

For fixed  $z_0$ , the phase shift  $\Delta\phi$  defined in (4) can be viewed as a potential function

$$\begin{aligned} \Delta\Phi(\cdot) : \mathbb{R}^2 &\rightarrow \mathbb{R}, \\ \mathbf{r}_{xy} &\mapsto \Delta\Phi(\mathbf{r}_{xy}). \end{aligned}$$

The set  $\Omega$  is defined as:

$$\Omega = \{ \mathbf{r}_{xy} \in \mathbb{R}^2 \mid |\Delta\Phi(\mathbf{r}_{xy})| \geq \beta \}, \quad (11)$$

where  $\beta$  is a positive constant less than the maximum of  $|\Delta\Phi(\mathbf{r}_{xy})|$ . As seen in Fig. 3, when  $\hat{n}$  lies in the  $\{x, y\}$  plane,  $\Omega$  consists of two symmetric subsets, each associated with one of the poles. These subsets are denoted  $\Omega^-$  ( $\Delta\Phi(\mathbf{r}_{xy}) < -\beta$ ) and  $\Omega^+$  ( $\Delta\Phi(\mathbf{r}_{xy}) > \beta$ ). When  $\hat{n}$  is normal to the  $\{x, y\}$  plane,  $\Omega$  is simply-connected and circular (right image in Fig. 4). The position and the shape of this set strongly depends on the position of the particle. Therefore, by tracking the boundary of  $\Omega$  the particle itself will be tracked. This means that the control law should ensure that the trajectory of the tip,  $\mathbf{r}_{xy}(t)$ , evolves in a neighborhood of the curve defined by  $|\Delta\Phi(\mathbf{r}_{xy}(t))| = \beta$ . Note that when  $\Omega$  is not simply connected there will be two possible trajectories; the final trajectory of the tip will depend on the initial conditions.

In this work we ignore the low level details of the control of the piezo actuators and instead focus on high-level trajectory determination. (See [20] for further details on control of the tip.) A basic model for the motion of the tip is:

$$\dot{\mathbf{r}}_{xy} = \begin{pmatrix} u \\ v \end{pmatrix}, \quad (12)$$

where  $u$  and  $v$  are the control actions. In order to achieve boundary tracking, the control law for (12) would rely on an estimate of the gradient of the potential field  $\nabla(\Delta\Phi)$ . However, in MFM the tip is evaluating the field point by point. To acquire an estimate of the gradient one would need to sample the field at three or more points which are not co-linear. This is very restrictive since it implies that the tip should move on complex trajectories in order to fulfill two tasks simultaneously- gradient estimation and boundary tracking. To overcome the difficulty of explicitly estimating the gradient, [1] proposes to introduce nonholonomic constraints on (12):

$$\dot{\mathbf{r}}_{xy} = V \begin{pmatrix} \cos(\theta) \\ \sin(\theta) \end{pmatrix} \quad (13a)$$

$$\dot{\theta} = \omega. \quad (13b)$$

With this approach it is possible to develop a control law which depends purely on the local geometry of the field. This enables one to analytically establish performance bounds related to the geometrical parameters of the potential field, and to quantify the limiting cases for the control. (For details see [1].) The control law chosen here is:

$$\omega = K_1 (|\Delta\Phi| - \beta) + K_2 \frac{d\Delta\Phi}{dt}, \quad (14)$$

where  $\frac{d\Delta\Phi}{dt}$  is the derivative of the phase difference evaluated along the trajectory of the tip. When the curvature of the boundary is nonzero, such a control law will not guarantee exact tracking but will stabilize the trajectory in some neighborhood of the boundary. In fact, since  $\Delta\Phi$  is locally radial near its critical points, there is a neighborhood  $\Lambda_p$  of  $\mathbf{r}_p$  such that:

$$\Delta\Phi(\mathbf{r}_{xy}) \approx f_p(\|\mathbf{r}_{xy} - \mathbf{r}_p\|), \quad \mathbf{r}_{xy} \in \Lambda_p, \quad (15)$$

where  $\mathbf{r}_p$  is the position of the critical point of the potential field and  $f_p$  is the radial function which approximates the potential function in the neighborhood  $\Lambda_p$ . The following theorem can be proved in case of unit speed ( $V = 1$ ):

*Theorem 1:* Consider the control law (14) applied to (13), when either  $\Omega^- \subset \Lambda_p$  or  $\Omega^+ \subset \Lambda_p$ . Let  $\mathbf{r}_d \in \Lambda_p$  be a solution of:

$$K_1 (|f(\|\mathbf{r}_d - \mathbf{r}_p\|) - \beta) + \frac{1}{\|\mathbf{r}_d - \mathbf{r}_p\|} = 0, \quad (16)$$

and let the gains  $K_1$  and  $K_2$  satisfy:

$$\left(\frac{K_2}{K_1}\right)^4 \frac{1}{4\|\mathbf{r}_d - \mathbf{r}_p\|^4} - \|\nabla(\Delta\Phi)\| \frac{K_2^2}{K_1} + 1 < 0, \quad (17)$$

where  $\|\nabla(\Delta\Phi)\|$  is evaluated for  $\mathbf{r}_{xy} = \mathbf{r}_d$ . Then if the initial conditions are such that

$$\left| K_1 (|f(\|\mathbf{r}_d - \mathbf{r}_p\|) - \beta) + \frac{1}{\|\mathbf{r}_d - \mathbf{r}_p\|} \right| < \delta_1 \quad (18a)$$

$$|\dot{\mathbf{r}}_{xy} \cdot \nabla(\Delta\Phi)| < \delta_2 \quad (18b)$$

where  $\delta_1, \delta_2 > 0$  are sufficiently small, the trajectory of the system converges to a level set defined by:

$$|\Delta\Phi(\mathbf{r}_{xy})| = -\frac{1}{K_1 \|\mathbf{r}_d - \mathbf{r}_p\|} + \beta. \quad (19)$$

*Proof:* See [1]. ■

Note that  $\frac{1}{\|\mathbf{r}_d - \mathbf{r}_p\|}$  is the curvature of the trajectory to which the system converges. Therefore from (19) and (16) it can be observed that the distance by which the trajectory will be offset from the boundary of  $\Omega$  will depend both on the magnitude of  $K_1$  and the curvature of the boundary.

### B. Control law implementation

We will divide the motion of the tip into three stages. In the first stage, the tip is scanned over the sample using a standard raster-scan pattern until the phase shift exceeds a pre-defined threshold,  $|\Delta\Phi| \geq \alpha$ . This event triggers the second stage, in which the desired trajectory of the tip is determined by (13) and (14). As discussed below, the parameters defining this trajectory are adapted to the particulars of the magnetic field of the sample (e.g. shape and gradient). During this transient process the tip gradually converges to a trajectory

with predefined radius. After converging, the third stage begins: tracking the motion of the particle.

The threshold  $\alpha$  completely characterizes the searching phase of the motion. The threshold should be chosen such that a desired probability of detection is achieved according to the noise model of (10).

The existence of the second stage is motivated by the fact that the interaction between the tip and the sample depends on many parameters which are in general either completely unknown or only estimated. These parameters include the orientation of the magnetization vector of the particle, the radius of the particle, the particle magnetization and the characteristics of the tip. In particular, for the approximation given by (15), the region enclosed by the tip's trajectory will be a circle with radius given by  $\|\mathbf{r}_d - \mathbf{r}_p\|$ . This radius will depend primarily on two factors: the structure of the magnetic field emanating from the sample and the chosen value of the parameter  $\beta$  in the control law (14). In order to compensate for the unknown details of the structure of the magnetic field, we introduce an additional feedback control to adjust  $\beta$ .

From (19), the relationship between  $\beta$  and  $\|\mathbf{r}_d - \mathbf{r}_p\|$  is:

$$\beta = f_p(\|\mathbf{r}_d - \mathbf{r}_p\|) + \frac{1}{K_1 \|\mathbf{r}_d - \mathbf{r}_p\|}, \quad (20)$$

where the steady-state trajectory is such that  $\mathbf{r}_{xy} = \mathbf{r}_d$ . This leads to the following adaptive strategy: choose gains  $K_1, K_2$ , such that given a minimum magnitude of the gradient  $\|\nabla(\Delta\Phi)\|$  and a critical radius of curvature  $R_c$ , the condition (17) is satisfied; then adapt  $\beta$  such that the trajectory satisfies:

$$\|\mathbf{r}_{xy} - \mathbf{r}_p\| = R_c. \quad (21)$$

From (20), taking into account that  $f_p$  is strictly decreasing in  $\Lambda_p$ , it can be inferred that  $\beta$  will be inversely proportional to  $\|\mathbf{r}_d - \mathbf{r}_p\|$ . Then, taking into account that the actual implementation of the control is done in the discrete domain, the control of  $\beta$  is given by:

$$\beta(k+1) = \beta(k) + K_3 (\|\mathbf{r}_{xy} - \mathbf{r}_p\| - R_c), \quad (22)$$

where the gain  $K_3$  is small enough, such that the overall trajectory remains stable.

The value of  $\|\mathbf{r}_{xy} - \mathbf{r}_p\|$  is not directly available as an input. It can be estimated from the control  $\omega$  using:

$$\|\mathbf{r}_{xy} - \mathbf{r}_p\|_{est} = \frac{1}{T} \sum_{i=k-T}^k \frac{V}{\theta(i) - \theta(i-1)}, \quad (23)$$

where sliding window average is used to filter out the error due to the thermal noise coming from the MFM and the deviation of the level sets from perfect circles.

## IV. SIMULATION RESULTS

In this section we present two simulations to illustrate the efficacy of the tracking approach. In each case the measurement bandwidth is fixed to  $B = 300$  Hz. From (10), the corresponding noise standard deviation in the phase measurement is  $\sigma_n = 0.196$  deg.

### A. Tracking a slowly-moving or fixed particle

In the first simulation, the speed of the particle is set small enough compared with the tip speed so that the particle can be treated as static. The tip velocity is fixed to  $V = 5$  nm/unit-time, where the notion of unit time can be interpreted as  $1/B$ . This yields an actual velocity of the tip of  $V_{actual} = 1.5$   $\mu\text{m/s}$ . The minimum value of the field gradient in the region, where the trajectory is supposed to evolve, was determined to be  $\|\nabla(\Delta\Phi)\| = 0.02$  deg/nm and we have chosen a critical curvature  $R_c = 50$  nm. From these parameters, the gains  $K_1$  and  $K_2$  are determined by (17) as  $K_1 = 0.2$  and  $K_2 = 2$ . Note that Theorem 1 assumes unit speed; the gradient and the curvature must be scaled by the speed  $V$ .

Fig. 5 shows the trajectory of the tip for a fixed particle and for a constant  $\beta = 0.7$  deg. The background of the figure corresponds to a standard MFM image acquired using a raster scan. The thermal noise is clearly evident in the image. The resulting  $|\Delta\phi|$  measured along the trajectory is shown in Fig. 6. The fluctuations in the filtered phase shift arise from the fact that the trajectory evolves in a region for which the assumption (15) is not valid (the level sets are not circles). As a result, the equilibrium condition in (19) changes along the trajectory.

Fig. 7 shows the trajectory of the tip when the adaptive control is implemented. As can be seen, the motion of the tip converges to a much more circular pattern. As a result the filtered value of  $|\Delta\phi|$  converges to a constant rather than oscillating (Fig. 8). The evolution of  $\beta$  is illustrated in Fig. 9.

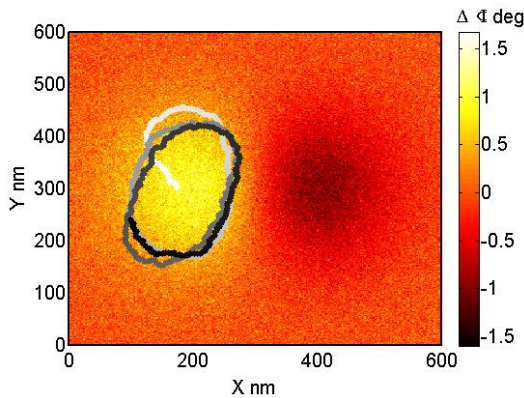


Fig. 5. The trajectory of the tip for  $\beta = 0.7^\circ$ . Trajectory colors correspond to time with the most recent points depicted in black.

### B. Tracking a moving particle

The motivating application of the algorithms presented in this paper is the study of the motion of single particles in molecular biology. Here, we consider a simulation based on the motion of a single influenza virus during the infection process. In [21], single-particle tracking techniques in wide-field epi-fluorescence microscopy were used to investigate the motion of single viral particles after endocytosis and through fusion to an endosome. The motion of the virus was shown to consist of three stages. The first stage occurred at the cell periphery and was quite slow with a typical speed of less than  $0.3$   $\mu\text{m/sec}$ . The second stage was a

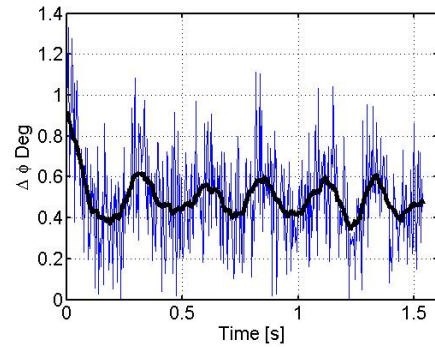


Fig. 6. The phase difference  $\Delta\phi$  measured along the trajectory. Both raw and filtered values are shown.

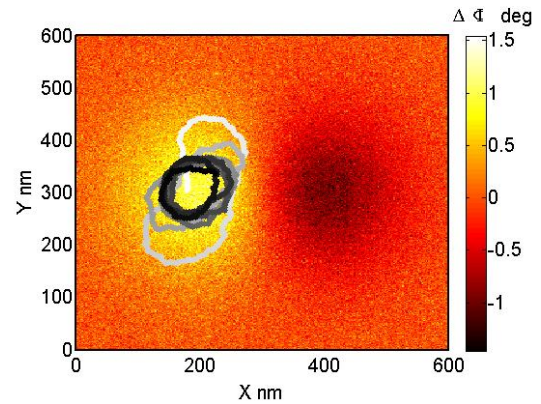


Fig. 7. The trajectory of the tip for when  $\beta$  is adapted according to (22). Trajectory colors correspond to time with the most recent points are depicted in black.

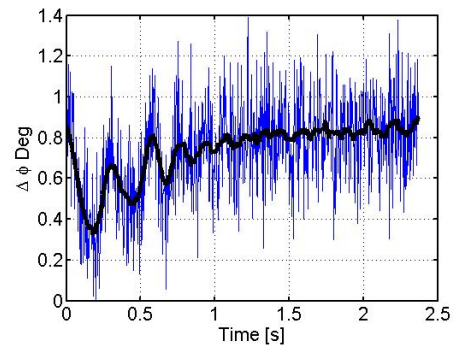


Fig. 8. The phase difference  $\Delta\phi$  along the trajectory in Fig. 7 (raw and filtered values).

rapid, unidirectional movement towards the nucleus with an average speed of about  $2$   $\mu\text{m/s}$ . The third stage occurred in the vicinity of the nucleus. This motion was once again relatively slow with typical speeds less than  $0.75$   $\mu\text{m/sec}$ .

Based on this, we simulated a two-stage motion of a magnetic particle similar to the first two stages of the influenza infection. The particle was static until  $t = 600$  ms at which time it started moving to the right at a speed of  $2.1$   $\mu\text{m/s}$ . To track this particle, the velocity of the tip was set to  $V = 15$  nm/unit-time, corresponding to  $V_{actual} = 4.5$   $\mu\text{m/s}$ . The critical curvature was selected to be  $R_c = 100$  nm

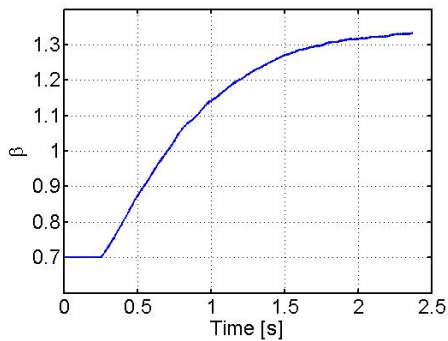


Fig. 9. The evolution of  $\beta$  according to (22) as the tip moves along the trajectory in Fig. 7.

and the gains were set to  $K_1 = 0.5$ ,  $K_2 = 2.4$ . The adaptive control law for  $\beta$  was executed while the particle was static. However, the speed of the particle during the second phase is comparable to the speed of the tip. As a result, the curvature of the tip trajectory is not directly related to the curvature of the level set. Therefore the adaptive control law was turned off during the second phase of motion. The resulting motion of the particle and the tip are shown at selected time instants in Fig. 10.

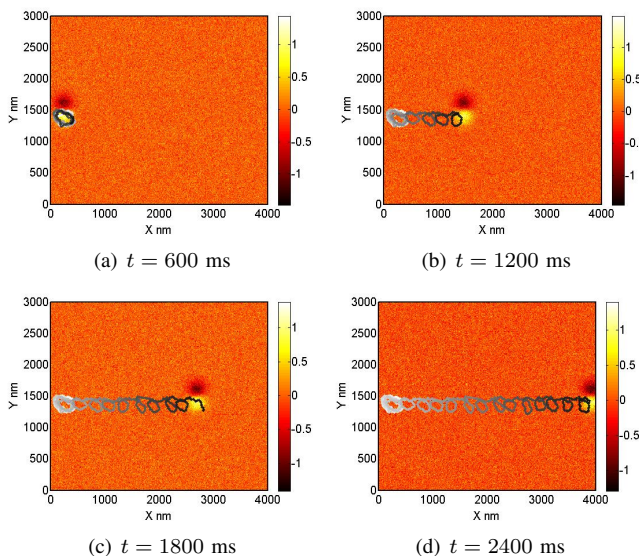


Fig. 10. Tracking a moving particle. The particle is fixed for the first 600 ms and then begins to move to the right at a velocity of  $2.1 \mu\text{m/s}$ . While the particle is fixed, the parameters  $\beta$  is adapted according to (22). Once the particle begins to move,  $\beta$  is held fixed. Trajectory colors correspond to time with the most recent points are depicted in black.

## V. CONCLUSIONS

In this paper we introduced a scheme for tracking nano-sized magnetic particles using an MFM. This scheme builds upon results from level-set tracking in potential fields and includes a parameter adaption to compensate for the details of the sample which are difficult to measure in practice. This is a preliminary investigation of the method and future work

will include analysis of its limitations, e.g. critical speeds for the tracked particle and critical signal-to-noise ratios. The next stage of our research is to move the control from the simulation realm into actual implementation and consecutively to build upon the current model to include sample topography, external interactions and other phenomena.

## REFERENCES

- [1] D. Baronov and J. Baillieul, "Reactive exploration through following isolines in a potential field," in *Proceedings of the American Controls Conference*, New York, NY, 2007, pp. 2141–2146.
- [2] Q. A. Pankhurst, J. Connolly, S. K. Jones, and J. Dobson, "Applications of magnetic nanoparticles in biomedicine," *J. Phys. D*, vol. 36, no. 13, pp. R167–R181, July 2003.
- [3] C. C. Berry and A. S. G. Curtis, "Functionalization of magnetic nanoparticles for applications in biomedicine," *J. Phys. D*, vol. 36, no. 13, pp. R198–R206, July 2003.
- [4] D. L. Graham, H. A. Ferreira, P. P. Freitas, and J. M. S. Cabral, "High sensitivity detection of molecular recognition using magnetically labelled biomolecules and megnetoresistive sensors," *Biosens. Bioelectron.*, vol. 18, no. 4, pp. 483–488, April 2003.
- [5] Y. Amemiya, T. Tanaka, B. Yoza, and T. Matsunaga, "Novel detection system for biomolecules using nano-sized bacterial magnetic particles and magnetic force microscopy," *J. Biotechnol.*, vol. 120, no. 3, pp. 308–314, November 2005.
- [6] U. Hartmann, "Magnetic force microscopy," *Annu. Rev. Mater. Sci.*, vol. 29, no. 1, pp. 53–87, 1999.
- [7] M. R. Kobischka and U. Hartmann, "Improving the lateral resolution of the MFM technique to the 10 nm range," *J. Magn. Magn. Mater.*, vol. 272–276, no. 3, pp. 2138–2140, May 2004.
- [8] G. Yang, J. Tang, S. Kato, Q. Zhang, L. C. Qin, M. Woodson, J. Liu, J. W. Kim, P. T. Littlehei, C. Park, and O. Zhou, "Magnetic nanowire based high resolution magnetic force microscope probes," *Appl. Phys. Lett.*, vol. 87, no. 12, p. 123507, September 2005.
- [9] G. Schitter, K. J. Astrom, B. DeMartini, G. E. Fantner, K. Turner, P. J. Thurner, and P. K. Hansma, "Design and modeling of a high-speed scanner for atomic force microscopy," in *Proceedings of the American Controls Conference*, Minneapolis, MN, 2006, pp. 502–507.
- [10] G. Schitter, P. Menold, H. Knapp, F. Allgöwer, and A. Stemmer, "High performance feedback for fast scanning atomic force microscopes," *Rev. Sci. Instrum.*, vol. 72, no. 8, pp. 3320–3327, August 2001.
- [11] G. Schitter, R. W. Stark, and A. Stemmer, "Fast contact-mode atomic force microscopy on biological specimen by model-based control," *Ultramicroscopy*, vol. 100, no. 3–4, pp. 253–257, August 2004.
- [12] G. Schitter, F. Allgöwer, and A. Stemmer, "A new control strategy for high-speed atomic force microscopy," *Nanotechnology*, vol. 15, no. 1, pp. 108–114, January 2004.
- [13] S. Salapaka, T. De, and A. Sebastian, "Sample-profile estimate for fast atomic force microscopy," *Appl. Phys. Lett.*, vol. 87, no. 5, p. 053112, August 2005.
- [14] S. B. Andersson and J. Park, "Tip steering for fast imaging in AFM," in *Proceedings of the American Controls Conference*, Portland, OR, 2005, pp. 2469–2474.
- [15] S. B. Andersson, "An algorithm for boundary tracking in AFM," in *Proceedings of the American Controls Conference*, Minneapolis, MN, 2006, pp. 508–513.
- [16] R. Engel-Herbert, D. Schaadt, and T. Hesjedal, "Analytical and numerical calculation of the magnetic force microscopy response: A comparison," *J. Appl. Phys.*, vol. 99, no. 113905, June 2006.
- [17] D. Rugar, H. J. Guethner, S. E. Lambert, J. E. Stern, I. McFadyen, and T. Yogi, "Magnetic force microscopy: General principles and applications to longitudinal recording media," *J. Appl. Phys.*, vol. 68, no. 3, 1990.
- [18] D. P. E. Smith, "Limits of force microscopy," *Rev. Sci. Instrum.*, vol. 66, no. 5, pp. 3191–3195, May 1995.
- [19] S. McVitie, R.P.Ferrier, J. Scott, G. White, and A. Gallagher, "Quantitative field measurements from magnetic force tips and comparison with point and extended charge models," *J. Appl. Phys.*, vol. 89, no. 7, April 2001.
- [20] D. Y. Abramovitch, S. B. Andersson, L. Y. Pao, and G. Schitter, "A tutorial on the mechanisms, dynamics, and control of atomic force microscopes," in *Proceedings of the American Controls Conference*, 2007, pp. 3488–3502.
- [21] M. Lakadamyali, M. J. Rust, H. P. Babcock, and X. Zhuang, "Visualizing infection of individual influenza viruses," *PNAS*, vol. 100, no. 16, pp. 9280–9285, July 2003.